Analysis of J-integral and HRR Singularity Using Experimental and Computational Hybrid Method with Image Processing

G. YAGAWA, N. SONEDA and S. YOSHIMURA
Department of Nuclear Engineering, University of Tokyo, 7–3–1, Hongo, Bunkyo-ku, Tokyo 113, Japan

ABSTRACT

This paper is concerned with the application of computer image processing technique to nonlinear fracture mechanics analyses. First, a new experimental and computational hybrid method to evaluate the J-integral is proposed. The displacement distribution near a crack tip is measured directly by means of the computer image processing technique. Then, the strain and the stress distributions are calculated, with which the J-integral is evaluated by the line integration technique. Since the method uses only the stress and strain values near the crack tip, the J-integral can be measured on arbitrarily shaped specimens.

The second application of the computer image processing here is the experimental evaluation of the HRR (Hutchinson-Rice-Rosengren) singularity field from the displacement distribution near the crack-tip.

To demonstrate the validity of these methods, a tensile test is performed on a compact specimen. Then, the J-integral values measured by the present method are compared with the Merkle-Corten equation. Also, comparing the experimental results with the numerical ones, the HRR singularity of the near-crack-tip is discussed in detail.

KEYWORDS

J-integral; HRR singularity; image processing; CT specimen; displacement measurement.

INTRODUCTION

In many occasions of assessing the integrity and safety of structures, nonlinear fracture mechanics have been widely utilized together with computer simulation techniques such as the finite element method. Especially, the J-integral (Rice, 1968) seems one of the most promising fracture mechanics parameters. The main reasons of this can be explained as follows. First of all, it has been proved theoretically that, under the conditions such that the deformation theory of plasticity is valid, the J-integral is directly related to the strength of the HRR (Hutchinson-Rice-Rosengren) singularity of the crack tip stress-strain fields (Hutchinson, 1968, Rice *et al.*, 1968), and also that it has a path independence (Rice, 1968). The latter characteristic is very convenient for the numerical evaluation of the J-integral. Another important fact is that, for some standardized shaped specimens, several simple experimental formulae which require only a load vs. load-point-displacement curve, have been developed (Beglay, 1972, Rice *et al.*, 1973, Merkle *et al.*, 1974).

Nevertheless, several problems still remain unsolved in the nonlinear fracture mechanics. First, the general procedure to measure the J-integral of arbitrarily shaped specimens has not been developed yet. For example, the simple experimental formula mentioned previously can be applied only to limited shaped specimens such as a three point bending specimen and a compact tension one. Even in the methods using strain gauges, the configuration of a specimen is restricted so that the partial differential of displacement

$\frac{\partial \varepsilon_y}{\partial x}$ may become zero or negligible at the location of strain gauges (Kawahara *et al.*, 1983, Frediani, 1984, Ohji *et al.*, 1985).

Second, the singularity has been rarely evaluated experimentally, though several numerical studies on the HRR singularity have been performed so far (Yagawa *et al.*, 1984, Shih, 1983).

The authors have developed a new optical method to directly measure the displacement distributions by means of the computer image processing (Yagawa *et al.*, 1984, 1985, 1987, Soneda *et al.*, 1988). In this study, the method is applied to the measurement of the J-integral as well as the HRR singularity field. In the evaluation of the J-integral, the strain and stress distributions near the crack tip are first calculated from the displacement distribution measured with the computer image processing. Then, the J-integral is calculated by the path integration technique, which is widely used in the finite element fracture analysis. Since this method uses only the stress and strain values near the crack tip, the J-integral can be measured on arbitrarily shaped specimens.

As for the HRR singularity, its dimensionless functions are evaluated experimentally with the measured displacement distribution near the crack tip and the J-integral.

To demonstrate the validity of these methods, a tensile test is performed on a compact tension (CT) specimen. The J-integral values measured by the present method are compared with those obtained with the Merkle-Corten's formula. Also, the experimental results of the dimensionless functions of the HRR singularity are compared with the numerical ones (Shih, 1983) in detail.

DISPLACEMENT MEASUREMENT SYSTEM BY MEANS OF COMPUTER IMAGE PROCESSING

Figure 1 shows the principle of the displacement measurement method (Yagawa *et al.*, 1984, 1985, 1987). First, hundreds of marks are printed on a surface of the specimen beforehand. Locations of marks are determined automatically by the computer image processing technique. The displacement of each mark is calculated as a difference between the locations of the mark before and after the deformation. The displacement distribution is calculated from the mark displacements using the data smoothing technique (Soneda *et al.*, 1988).

Figure 2 shows the hardware of the present image processing system. A vidicon camera is used as an image input device. A TV image has 1024 times 1024 pixels. The brightness of a pixel is expressed by 256 digital gray levels. The host computer used here is a 16-bit personal computer (NEC PC-9801).

In general, it takes tremendous time for the personal computer to process the image data of one mega-bytes ($1024 \times 1024 \times 8$ bits) as above. In order to shorten the processing time, the image processing algorithm is divided here into two stages.

In the first stage, named 'Pre-processing', low density image data of 256×256 pixels are used. The algorithm of the pre-processing is shown in fig. 3. High-frequency noises in the image are taken off in the 'SMOOTHING' process. The change of the gray level of mark is sharpened in the 'ENHANCEMENT' process. The shading in the background of the image is removed in the 'LAPLACIAN' process. The gray image is converted to a binary image in the 'BINARIZATION' process. Finally, rough locations and sizes of marks are determined by tracing their boundaries in the 'BOUNDARY FOLLOWING' process.

In the second stage, named 'Main-processing', so-called windows are set in the original fine image. The precise location of each mark is determined in the window as the central coordinate of the gravity of the mark.

After these image processing processes, the smoothing technique developed by the analogy with the concept of the Sobolev-norm (Shih, 1984) is applied to the data of the mark displacements in order to reduce the measurement errors and to obtain the smooth displacement distribution (Soneda *et al.*, 1988). The measured area A is subdivided into a number of four-noded finite elements, and then the nodal values of the displacement vector $\mathbf{u}$ are determined by minimizing the following error measure ϕ:

$$\phi = \int_A (\mathbf{u} - \overline{\mathbf{u}})^2 dA + \int_A (\mathbf{u}' - \overline{\mathbf{u}}')^2 dA \tag{1}$$

where $\overline{\mathbf{u}}$ are the vector of the measured displacements of marks, and the prime denotes the first-order derivative with respect to the coordinate. Using this technique, the smooth distributions of both the displacement and its derivative can be obtained.

EVALUATIONS OF J-INTEGRAL AND HRR SINGULARITY

As mentioned previously, the image processing technique is utilized to directly measure the displacement distribution near the crack tip. In this section, the procedures of the J-integral as well as the HRR singularity evaluations from the displacement distribution will be described in detail.

J-integral by Line Integration

Considering the Cartesian coordinate system and the integration path Γ , the J-integral is defined as follows :

$$J = \int_\Gamma (W n_1 - T_i \frac{\partial u_i}{\partial x}) d\Gamma \tag{2}$$

where Γ is an arbitrary path sorrounding the crack tip, n_1 the x_1 component of the outward normal vector on Γ and $T_i (= \sigma_{ik} n_k)$ the traction force applied on Γ, respectively. The strain energy density W is defined as :

$$W = \int_0^{\varepsilon_{ij}} \sigma_{ij} d\varepsilon_{ij} \tag{3}$$

where σ_{ij} and ε_{ij} are the stress and strain tensors, respectively.

In the present method, the J-integral is evaluated through the numerical integration of eq. 2 just like the usual finite element fracture analysis. The strain distribution is calculated by multiplying the differential matrices to the displacement vectors for all the elements. Then, the corresponding stress distribution is calculated, assuming an appropriate constitutive equation of material. In general, the incremental theory of plasticity is considered to be more suitable for describing the actual elastic-plastic deformation process involving loading, unloading and reloading than the deformation theory of plasticity. However, in many situations such as the standardized fracture toughness tests under a monotonic loading condition, such history effects can be neglected, and the deformation theory of plasticity remains to be valid.

In this case, the total stress tensor σ_{ij} is directly related to the total strain tensor ε_{ij} through the following nonlinear equation :

$$\sigma_{ij} = \frac{2G}{1 + 3G/H_s} (\varepsilon_{ij} + \frac{\nu + (1+\nu) G/H_s}{1 - 2\nu} \delta_{ij} \varepsilon_{mm}) \tag{4}$$

where G is the elastic shear modulus, H_s the plastic secant modulus, ν the Poisson's ratio and δ_{ij} the Kronecker's delta, respectively. H_s is written in terms of both Mises type equivalent stress $\overline{\sigma}$ and equivalent plastic strain $\overline{\varepsilon^p}$ as :

$$H_s = \frac{\overline{\sigma}}{\overline{\varepsilon^p}}. \tag{5}$$

In the present study, the stress tensor is calculated, solving eq. 4 by the Newton-Raphson method.

Since the strain and the stress tensors are obtained at Gauss integration points in each finite element, the J-integral is eventually evaluated numerically by the path integration technique, which is popular in the finite element fracture analysis.

HRR Singularity

For the material of a pure power-law type uniaxial stress-strain relation as :

$$\frac{\varepsilon}{\varepsilon_0} = \alpha (\frac{\sigma}{\sigma_0})^n, \tag{6}$$

the HRR singularity of the near-tip displacement field is written as follows :

$$u_i = \alpha \varepsilon_0 (\frac{J}{\alpha \varepsilon_0 \sigma_0})^{\frac{n}{n+1}} r^{\frac{1}{n+1}} F_i(\theta, n), \quad i = r, \theta \tag{7}$$

where u_i is the displacement, r and θ the polar coordinates centered at the crack tip, ε_0 the yield strain, σ_0 the yield stress, n the hardening exponent, α the material constant and $F_i(\theta, n)$ the dimensionless function, respectively (Hutchinson 1968, Rice *et al.*, 1968)

In the present study, F_r and F_θ are calculated from the nodal displacement $u_i(r, \theta)$ at a location (r, θ) and the J-integral as follows :

$$F_i(r, \theta) = \frac{u_i(r, \theta)}{\alpha \varepsilon_0 (\frac{J}{\alpha \varepsilon_0 \sigma_0})^{\frac{n}{n+1}} r^{\frac{1}{n+1}}}, \quad i = r, \theta \tag{8}$$

EXPERIMENT

To demonstrate the validity of the methods, they are applied to a CT specimen under tensile load.

Experimental Procedure

Figure 4 shows the configuration and the dimensions of the CT specimen made of Type 304 stainless steel, in which a mechanical notch is machined and then a fatigue precrack is given up to a length of a=115mm. Figure 5 illustrates the multi-linear approximation of the experimental data of a uniaxial stress-strain relation of this material. Also, the same experimental data can be curve-fitted by the Ramberg-Osgood's type constitutive equation as :

$$\frac{\varepsilon}{\varepsilon_0} = \frac{\sigma}{\sigma_0} + \alpha(\frac{\sigma}{\sigma_0})^n. \tag{9}$$

where ε_0, σ_0, α and n are 0.00126, 234MPa, 3.15 and 5, respectively.

Several hundreds of small marks, whose diameter and distance are 0.13 and 0.25mm, respectively, are printed on the specimen surface by means of the photo-chemical etching technique. Using a servo-hydraulic MTS machine, a displacement-controlled loading is applied statically to the specimen at a room temperature. The load vs. load-point-displacement curve is recorded for the sake of the J-integral evaluation by the Merkle-Corten's formula (Merkle *et al.*, 1974). At several loading stages, the load is held for a while to take a picture of the crack tip region. The pictures are processed after the experiment.

Strain Distribution

Figure 6 shows the measured load vs. load-point-displacement curve. The pictures of marks around the crack tip are taken at three loading stages of δ = 1.5, 2.0 and 4.0mm, respectively. Figure 7 shows the picture taken at the load-point-displacement δ of 2.0mm. In the rectangular region in fig. 7, the strain, the stress, the J-integral and the HRR singurality are calculated using the marks and the four-noded finite element mesh as shown in fig. 8.

Figure 9 shows the contours of the equivalent strain corresponding to fig. 7 and five integration paths used for the J-integral evaluation. The sizes of the integration paths range from 1 to 3mm. It can be seen from the figure that the strain value is concentrated near the crack tip.

J-integral

Figure 10 shows the J-integral values plotted against the path number at two loading stages of step 1 and 2, respectively. The open circles denote the J-integral values J_p evaluated by the present method and the dashed line the J-integral values J_m by the Merkle-Corten's formula, respectively. It can be seen from the figure that, at both stages, J_p holds the good path independence, and also that J_p and J_m agree well with each other at step 1, while J_p is by 10 to 20% less than J_m at step 2.

Figure 11 shows the J-integral vs. load curve, where the solid line denotes J_m, and the dashed line and the error bar denote the mean value and the maximum difference of the J_p values, respectively. The figure clearly demonstrates that J_p and J_m agree well when the loading level is low, and their difference increases gradually with the loading level.

Figure 12 shows the J-integral vs. CTOD curve. Here, the CTOD is defined as a change of the distance between the marks A and A' in fig. 8. In fig. 12, the J_p and CTOD values have a fairly proportional relationship as expected from the fracture mechanics theory (Shih, 1981). However, the J_m has not a linear relation with CTOD as shown in the same figure.

These slightly different features between J_p and J_m are considered to be mainly caused by the three dimensional effects of through-wall cracks as discussed later.

Crack Tip Singularity

The crack tip singularity is studied here based on the crack tip displacement distribution. Figures 13 and 14 show the comparison between the experimental and numerical results of the dimensionless functions. In both figures, each symbol '+' denotes the experimental results of F_r^e and F_θ^e at step 1, which are obtained as nodal values of the finite element mesh. The solid and broken lines denote the numerical results of F_r^a and F_θ^a calculated under either plane strain or plane stress conditions, respectively (Shih, 1983). It can

be seen from the figures that the experimental and numerical curves are similar to each other in shape, whereas their magnitudes are a little different.

DISCUSSIONS

It is confirmed from the experiment described in the previous sections that the present method based on the image processing technique is effective in evaluating the J-integral as well as the crack tip singularity. However, there is still some inconsistency between the experimental results and the theoretical presumption. It seems that this inconsistency is mainly caused by the three-dimensional effects of the crack.

To begin with, let us examine the evaluation procedures of the J-integral. It is well known from several three-dimensional studies on through-wall cracked specimens that the J-integral value is usually smaller on the specimen surface than inside (Kikuchi *et al.*, 1983, Wellman *et al.*, 1985). The value in the experiment in the previous section, J_p, is evaluated using the strain and stress values measured on the specimen surface near the crack tip, while J_m evaluated from the Merkle-Corten's formula is based on the load vs. load-point-displacement curve. From this consideration, it is easily expected that the present scheme by the computer image processing evaluate the J-integral on the specimen surface, while the simple experimental formula as that of Merkle-Corten does the average value of the J-integral along the crack front. This may be the main reason why J_p is a little smaller than J_m in fig. 11 at higher loading levels.

The reason why F_r^e and F_θ^e disagree in a qualitative sence with either of the two-dimensional numerical results as shown in figs. 13 and 14 may be also attributed to the fact that the experimental results are measured on the specimen surface.

It is noted that the J_p and CTOD values have a good proportional relationship on the specimen surface (see Fig. 12) and that, irrespective of the loading level, the identical dimensionless functions are obtained using both J_p and the near crack tip displacement distribution on the specimen surface. These results seem to predict that there could be a singularity field on the surface, slightly different from solutions obtained from the two-dimensional analyses.

To study these three-dimensional effects more precisely, the further experiments and the three-dimensional numerical simulation are strongly required.

CONCLUSIONS

The conclusions obtained in this study are given as follows :

(1) The J-integral is successfully obtained using the displacement distribution near the crack tip measured by the computer image processing technique. The main advantage of the method is the capability in evaluating the J-integral of arbitrarily shaped specimens since the method uses only information near the crack tip.
(2) The singularity of the crack tip displacement field is evaluated experimentally.
(3) There could be a special singularity field on the specimen surface, slightly different from the two-dimensional numerical results.

ACKNOWLEDGEMENT

This work was performed with a financial support from the Grant-in-Aid for the research of the Ministry of Education, Science and Culture.

REFERENCES

Begley, J.A. and Landes, J.D. (1972). The J-integral as a fracture criterion in fracture toughness testing, *ASTM STP 514*, 1-39.

Frediani, A. (1984). Experimental measurement of the J-integral, *Eng. Fract. Mech.*, 19, 1105.

Hutchinson, J.W. (1968). Singular behavior at the end of a tensile crack in a hardening material, *J. Mech. Phys. Solids*, 16, 13-31.

Kawahara, W.A. and Brandon, S.L. (1983). J-integral evaluation by resistance strain gauges, *Engrg. Fract. Mech.*, 18, 427-434.

Kikuchi, M., Miyamoto, H. and Tanaka, M. (1983). J integral evaluation of CT specimen in elastic-plastic state, *Trans. JSME*, 50, 463-470, (in Japanese).

Merkle, J.G. and Corten, H.T. (1974). A J-integral analysis for the compact specimen, considering axial force as well as bending effects, *Trans. ASME, J. Press. Ves. Tech.*, 94, 286-292.

Ohji, K., Kubo, S., Tsuji, M. and Miyamoto, S. (1985). Nondestructive evaluation of crack length and stress intensity factor by means of J and M integrals, *Trans. JSME*, 51, 1263-1270 (in Japanese).
Rice, J.R. (1968). A path independent integral and the approximated analysis of strain concentration by notchs and cracks, *Trans. ASME, J. Appl. Mech.*, 35, 379-386.
Rice, J.R. and Rosengren, G.F. (1968). Plane strain deformation near a crack-tip in a power-law hardening material, *J. Mech. Phys. Solids*, 16, 1-12.
Rice, J.R., Paris, P.C. and Merkle, J.D. (1973). Some further results on J-integral analysis and estimates, *ASTM STP 536*, 231-245.
Shih, C.F. (1981). Relationship between the J-integral and the crack-opening displacement for stationary and existing cracks, *J. Mech. Phys. Solids*, 29, 305-326.
Shih, C.F. (1983). Tables of Hutchinson-Rice-Rosengren singular field quantities, *MRL E-147, Brown University.*
Shih, T.M. (1984). Numerical heat transfer, *Hemisphere Publishing Corporation*, 505.
Soneda, N., Yoshimura, S., Yoshioka, A. and Yagawa, G. (1988). Data smoothing technique using finite elements and Sobolev norm, *Trans. JSME*, 54, 1354-1358, (in Japanese).
Wellman, G.W., Rolfe, S.T. and Dodds, R.H. (1985), Three-dimensional elastic-plastic finite element analysis of three-point bend specimens, *ASTM STP 868*, 214-237.
Yagawa, G and Aizawa, T. (1984). A superposition method for nonlinear crack problems, *ASTM STP 803*, I-354-369.
Yagawa, G. and Matsuura, S. (1984). Strain distribution around a crack tip in high temperature environment using picture processing, *Nucl. Engrg. Des.*, 83, 259-265.
Yagawa, G. and Yoshimura, S. (1986). On the dynamic fracture toughness and crack tip strain behavior of nuclear pressure vessel steel : application of electromagnetic force, *Nucl. Engrg. Des.*, 97, 195-209.
Yagawa, G. and Soneda, N. (1987). Application of computer picture processing to dynamic strain measurement under electromagnetic field, *Proc. Int. Conf. on 9th SMiRT, B*, Lausanne, 19-24.

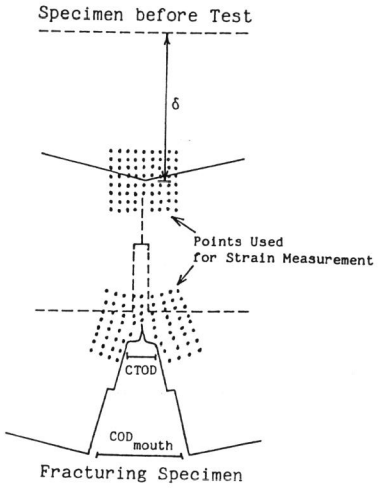

Fig. 1 Marks around a crack tip before and after deformation.

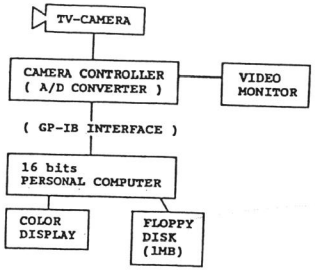

Fig. 2 Hardware of image processing system.

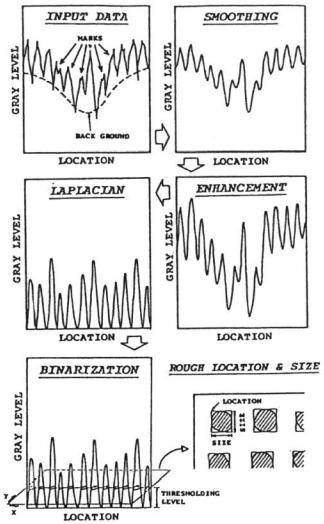

Fig. 3 Algorithm of pre-processing.

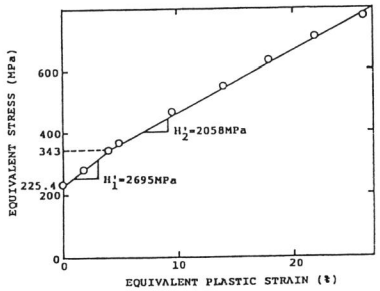

Fig. 5 Uniaxial stress-strain relation of Type 304 stainless steel.

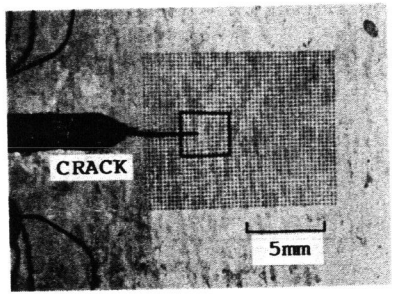

Fig. 7 Picture of marks at step 1.

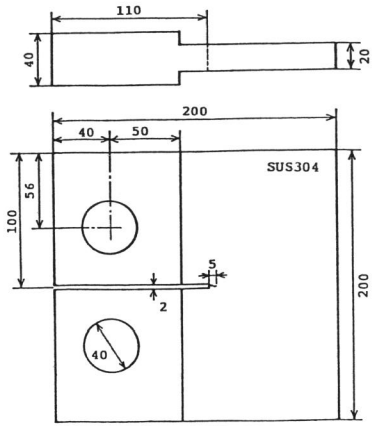

Fig. 4 Configuration and dimensions of CT specimen.

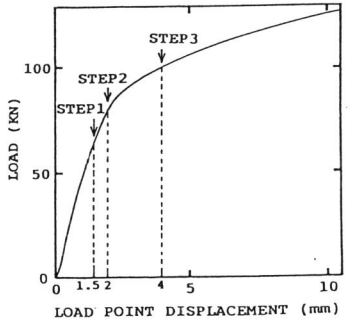

Fig. 6 Load vs. load-point-displacement curve.

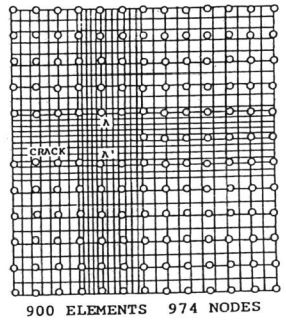

Fig. 8 Mark locations and overlapped finite element mesh.

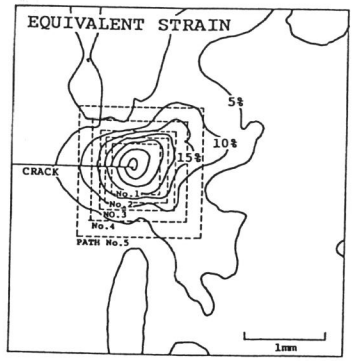

Fig. 9 Equivalent strain distribution.

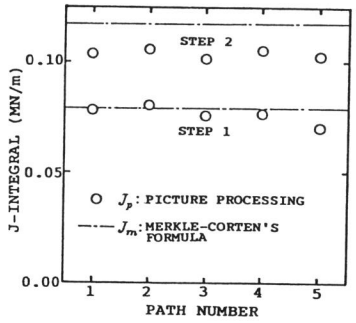

Fig. 10 J-integral distribution plotted against path number.

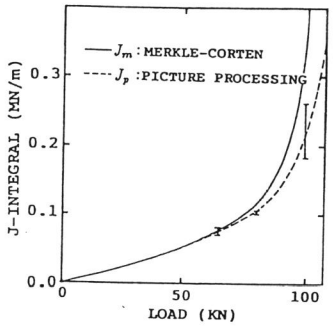

Fig. 11 J-integral vs. load curve.

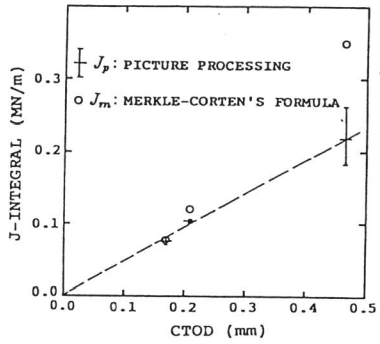

Fig. 12 J-integral vs. CTOD curve.

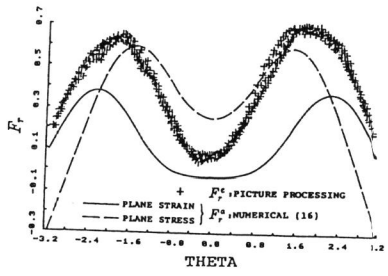

Fig. 13 Comparison between experimental and numerical results of F_r at step 1.

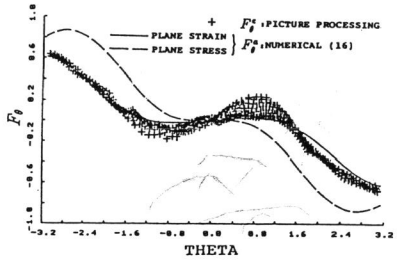

Fig. 14 Comparison between experimental and numerical results of F_θ at step 1.